Using Very High Resolution (VHR) imageries within a GEOBIA framework for gully mapping: an application to the Calhoun Critical Zone Observatory

A. Francipane[1], G. Cipolla[1], A. Maltese[1], G. La Loggia[1], L.V. Noto[1]

[1] Dipartimento di Ingegneria (DI), Università di Palermo, Viale delle Scienze, 90142 Palermo, Italy

Abstract

Gully erosion is a form of accelerated erosion that may affect soil productivity, restrict land use, and lead to an increase of risk to infrastructure. Although an accurate mapping of these landforms is important, such an activity can be difficult because of the presence of dense canopy, which precludes the identification through aerial photogrammetry and other traditional remote sensing methods, and/or the wide spatial extent of some gullies, which makes their identification and characterization through field surveys a very large and expensive proposition. Even where possible, mapping of gullies through conventional field surveying can be an intensive and expensive activity. One cheaper and more expeditious way to detect gullies can be achieved in terms of morphological characteristics derived by Digital Elevation Models (DEMs). Moreover, the recent widespread availability of Very High Resolution (VHR) imagery, such as Laser Imaging Detection and Ranging (LIDAR) data, has led to a remarkable growth in the availability of terrain information providing a basis for the development of new methodologies for analyzing Earth surfaces.

This work aims to develop a geographic object-based image analysis to detect and map gullies based on a set of rules and morphological characteristics retrieved by a VHR imagery. A one-meter resolution LIDAR DEM is used to derive different morphometric indices, which are combined, by using different segmentation and classification rules, to identify gullies. The tool has been calibrated using, as reference, the perimeters of two relatively large gullies that have been measured during a field survey in the Calhoun Critical Zone Observatory (CCZO) area in the Southeastern United States. The developed procedure has been then applied and tested on a greater area, corresponding to the Holcombe's Branch watershed within the CCZO. Results were compared to previous works conducted over the same area demonstrating the consistency of the developed procedure.

1. Introduction

Overland flow erosion can be considered as a threshold process occurring only after resistance forces are exceeded (Francipane et al., 2012; Huggett, 1990). Entity and evolution of this phenomenon depend on several factors such as the hydrological regime, the geomorphological characteristics, the climate, and the land use of the basin (Francipane et al., 2015; Nearing et al., 1999; Pimentel et al., 1995; Wilkinson and McElroy, 2007). All of these factors are related to each other and determine, to a different degree, the extent of the erosive process, changes on soil productivity, landscape evolution, and its variations in space and time (Henderson-Sellers, 1994; Kirkby and Cox, 1995).

Erosion typically starts as a series of subparallel rills parallel to the slope gradient. Slight variations in surface topography can produce greater depth of flow, resulting in increased erosive forces and in an accelerated erosion, which promotes the evolution of rills into more severe forms of erosion: the gullies (Ritter et al., 2011). The formation of gullies is highly sensitive to changes in the factors that control erosion and can be exacerbated from absence of vegetation, agricultural practices, low cohesion in soil, or more generally, by all those practices that lower resistance and infiltration capacity of soils. In some cases these landforms can make difficult the use of heavy equipment needed for plowing and harvesting, thus restricting land use of an area, and increase risk to infrastructure (Noto et al., 2017; Ritter et al., 2011). According to Poesen et al. (2003), the total soil losses caused by gully erosion could rise up to 90% in different parts of the world. For all of these reasons, gully erosion and their identification in the territory have always attracted the interest of the scientific community (Valentin et al., 2005).

First attempts to study gullies go back to the 1930s, when Ireland et al. (1939) tried to study and describe the conditions governing the development of gullies in the Piedmont of South Carolina. In 1960s, Tuckfield (1964) described the processes that led to the formation of gullies in the New Forest of Hampshire (England) and Seginer (1966) presented different methods to quantify gully erosion. In 1977, the Soil Conservation Service (SCS, 1977) used a multivariate analysis to predict the gully growth, while Stocking (1980) used multiple regression analysis to predict gully-head retreat on 66 gullies in Zimbabwe.

The advent of digital elevation models (DEMs) led to the born and diffusion of quantitative land-surface analysis (i.e., geomorphometry) (Grosse et al., 2012). For many years, the main problem

related to the use of DEMs for land-surface analysis has been their relatively low spatial resolution. The issue seems to be overcome with the advent of very high-resolution (VHR) imageries, which started with the launch of IKONOS in 1999 and which finds nowadays its maximum expression in LIDAR data, that allows to derive very high resolution Digital Surface Models (DSMs) and bare ground DEMs. These products, which constitute a basic support for activities such as the hydrological-hydraulic modeling and the identification of areas exposed to flood risk, have provided the opportunity to develop new methodologies for analyzing Earth surfaces (Tarolli et al., 2009) that have found a widespread use also in identifying the scares of gullies in landscape in the last decade (Francipane et al., 2018; Jackson et al., 1988; James et al., 2007; Noto et al., 2017; Ritchie et al., 1994).

So far today, there are mainly two different procedures to deal with high-resolution DEM: a per-pixel approach (pixel-based) and a per-object approach (object-based). The last one is often referred to as Object Based Image Analysis (OBIA or GEOBIA if it takes into account the GEographical aspect as well). While the pixel-based approach uses the classical rules of map algebra applied to the pixel, the object-based approach uses the concept of the image object. The second approach releases on the definition of objects as a group of neighbor pixels with similar characteristics. The main advantage of such an approach is that object characteristics (e.g., mean value, standard deviation, ratio, etc.) and features (e.g., shape and texture) can be calculated and used to differentiate land cover classes with similar spectral information. These extra types of information give OBIA the potential to produce classifications characterized by accuracies higher than those produced by traditional pixel-based method. According to Boardman (2006), which says that field detection and measurements of gullies are very accurate but can be feasible only at small scale, this new technique could be the only practical approach to detect very extensive gullies in large areas (Knight et al., 2007).

One of the earlier efforts in detecting gullies by means of OBIA technique was made about ten years ago by Eustace et al. (2009). The authors developed a semi-automated method to predict the presence and volume of gullies for unsampled locations within the Fitzroy catchment into the Great Barrier Reef lagoon, on the east coast of Australia. They used data from twenty LIDAR transects acquired in 2007. Shruthi et al. (2015) conducted a study with the aim of quantifying temporal changes in gully system areas applying the OBIA to a 1-meter resolution DEM obtained from the IKONOS mission. The authors were successful in achieving the gullies by developing a set of

improved rules based on the knowledge of gully landform and process related to their formation. D'Oleire-Oltmanns et al. (2014) put together the GEOBIA analysis and the expert knowledge to set up an ensemble of rules to delineate gullies. They used as input a multispectral QuickBird 2 satellite image and calculated the accuracy by comparing the results of their classification with the reference data obtained by field surveys. After an initial multi-resolution segmentation, assigning different weights to the visible (RGB) and near infrared (NIR) bands, the authors detected the gully-affected areas through a 3-step classification. First of all, they extracted large homogeneous areas (i.e., plantations, residential areas). Then, they detected the gully-affected areas basing on the shadow of the Sun-diverted gully walls, which presents a spectral contrast between the surrounding surface and the sunlit opposite gully walls (D'Oleire-Oltmanns et al., 2014). The last step consisted of the removal of false positives to make more acceptable the results of the previous analysis. Yang et al. (2017) developed and applied a multidirectional hill-shading method to extract gullies with an OBIA approach. The approach allowed the authors to get boundaries of gullies with high location accuracy and solve the discontinuity and low location accuracy caused by the pixel-based methods. Rahmati et al. (2017) put in evidence that the GEOBIA technique is less expensive than any other approach to detect gullies, such as soil erosion measurements, especially over the last few years because it leads to the highest values of accuracy. In their paper, gully erosion mapping was performed using a DEM, a SPOT-5 panchromatic satellite image, and a Multi-Resolution segmentation.

Starting from knowledge about morphology and geomorphological processes leading to gullies, this paper aims to develop a set of rules about morphometric aspects and processes related to the formation of these landforms for the identification of gullies within a GEOBIA framework. The framework is applied to the Calhoun Critical Zone Observatory where several gullies have been observed and mapped by other studies (James et al., 2007; Noto et al., 2017) and where a very high resolution (i.e., 1 m) LIDAR DEM is available. The procedure, firstly calibrated for two gullies detected during a field survey carried out in June 2015, will be applied to the CCZO and results compared to those obtained by Noto et al. (2017). The framework has been developed within the software *eCognition developer 9.2* (Trimble Geospatial).

2. Study area and dataset: The Calhoun Critical Zone Observatory

The Calhoun Critical Zone Observatory (CCZO) is located in South Carolina (US) and is part of the Critical Zone Observatory (CZO) project, which involves different institutions with the main goal to study and understand the processes that shape the surface of Earth and support terrestrial life.

The CCZO is a particularly interesting site for studying gully erosion since after more than a century of intensive crop production; terrains were abandoned and experimented a severe process of erosion that has led to the loss of almost 20 cm of top soil with the formation of numerous gullies. Today, the gullies are mainly blanketed by reforestation, but the scars of these particular landforms are still present. More details about this area can be found in James et al. (2007).

With reference to the data, LIDAR DEM was obtained by the study of Noto et al. (2017). Following the same work scheme of Noto et al. (2017), a first area (SUBAREA-A) of about 1 km^2 was used to develop the GEOBIA procedure, while a second area (SUBAREA-B) with an extension of about 4.3 km^2, corresponding to the Holcombe's Branch watershed, was used to test the developed procedure. The SUBAREA-A, in particular, contains two gullies surveyed during a field survey carried out in June 2015 that were used to calibrate the GEOBIA procedure. Figure 1 shows the LIDAR DEM for the SUBAREA-A (left part of the figure) and the SUBAREA-B (right part of the figure). Detailed information about the data and the two sub-areas can be found in Noto et al. (2017).

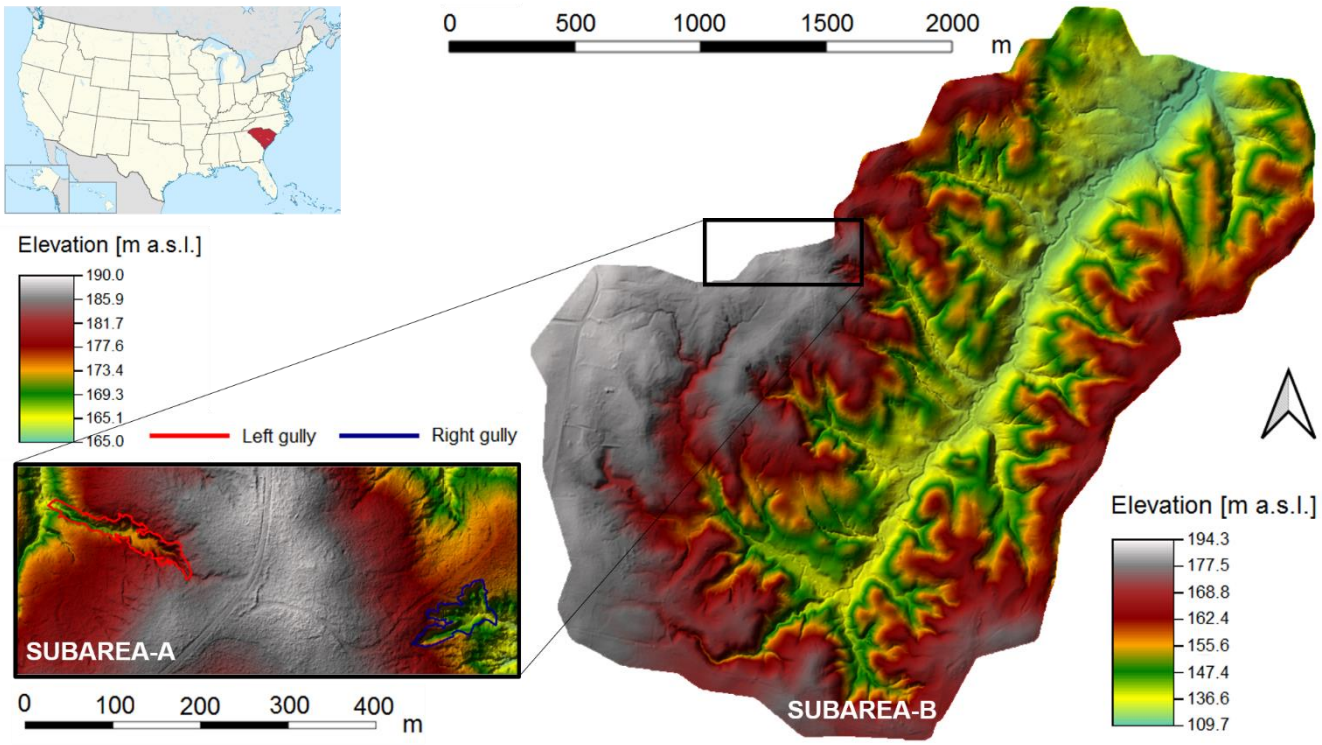

Figure 1 – LIDAR DEM of the SUBAREA-B (Holcombe's Branch watershed) of the CCZO (on the right) and focus on the SUBAREA-A (on the left) containing the two gullies (left gully in red and right gully in blue) surveyed and used for the calibration of the GEOBIA procedure.

3. Methods

The methodology builds on the use of four different morphometric indices able to detect the presence of specific landforms, which can be interpreted as part of a gully (bottom and edges): the Topographic Position Index (*TPI*), the terrain slope, the roughness slope, and the length to width ratio. In particular, three of them have been derived with classical pixel-based procedures, while the remaining index with an object-based approach. In particular, only the TPI has been used to detect the internal part of gully, while the remaining three to identify the gully boundary (i.e., terrain slope, roughness slope, and length to width ratio).

The Section 3 is organized as follows. Section 3.1 provides a brief description of the aforementioned indices. Section 3.2 summarizes the OBIA procedure developed to identify gullies within the SUBAREA-A with particular reference to the two main phases of OBIA: segmentation and its calibration (Section 3.2.1) and classification (Section 3.2.2).

3.1. Morphometric indices

3.1.1. *TPI* for gully bottom

The *TPI* (Guisan et al., 1999; Jenness, 2006) is defined as the difference between the elevation of a central pixel, z, and the mean elevation, $\bar{z}_\alpha$, of its surrounding cells within the kernel of size α. Negative values mean the cell is lower than its surroundings. If z is significantly lower than $\bar{z}_\alpha$, which implies significant low values of *TPI*, then the cell is likely at or near the bottom of depression (e.g., the bottom of a valley or a gully). In particular, we used the normalized *TPI* (*nTPI*) by dividing by the mean value of elevation within the used kernel:

$$nTPI_\alpha = \frac{(z-\overline{z_\alpha})}{\overline{z_\alpha}}, \quad (1)$$

Since the *TPI* is kernel-dependent, in order to decide the size of the kernel to use, we used different kernel size α (see Section 3.2). The $nTPI_\alpha$ was calculated in QGIS (QGIS Development Team, http://qgis.org) starting from the existing GRASS *r.neighbors* function.

3.1.2. Terrain slope for gully edge

Terrain slope, which is the first spatial derivative of the terrain elevations, is one of the basic terrain parameters widely used in terrain analysis and landform classification. Slope has been here adopted as index of gully edge presence since the gully edges can be assimilated to abrupt changes of slope in the terrain (Liu et al., 2017; Shruthi et al., 2011). It was obtained in QGIS from the LIDAR DEM through using the existing GRASS *r.slope.aspect* tool.

3.1.3. Terrain roughness for gully edge

Terrain roughness is a morphometric measure expressing the local heterogeneous of terrain. Since a DEM-derived roughness characterizes the local variance of surface gradients, distinguishing between smooth and rugged landforms, might be a useful indicator of gully edge presence (Liu et al., 2017). The terrain roughness can be defined in several differing ways, depending on the field of study, the scale of analysis, and the aim of application (Milenković et al., 2015). According to Liu et al. (2017), here the terrain roughness is defined as the inverse of the cosine of slope angle. It was obtained using equation (2) within the *raster calculator* of QGIS:

$$r = \frac{1}{\cos(slope)}. \quad (2)$$

Since the roughness is directly derived from slope, in order to verify that the information provided by the terrain roughness is not redundant in detecting the edges of gullies, some tests for the SUBAREA-A have been carried out. The results of the tests, which will not be here shown for the sake of brevity, demonstrated that considering this variable reduces the number of false positives, i.e., non-gully segments assigned to the class *gully edge*. For this reason, it was decided to include also this topographic feature in the process of edges' detection. Moreover, this choice is strengthened by Liu et al. (2017), where both the terrain slope and roughness have been used to detect edges, obtaining high accuracy values as well.

3.1.4. Length to width ratio for gully edge

Since gullies are usually tiny and long landforms whit flat bottoms and edges with changeable gradients, in an object-based procedure, elements representing the edges are likely to have one of the two dimension higher than the other one (D'Oleire-Oltmanns et al., 2014; Eustace et al., 2009). This information is contained within the length to width ratio, which gives an indication of the compactness of an element. In particular, values of length to width ratio greater than one means that the object is longer in one of its two dimensions. The index has been obtained in *eCognition developer 9.2*, which will be shortly described in the following.

3.2. Description of gully detection within a GEOBIA framework

The developed procedure can be summarized in the flow charts of Figure 2. The first step of the object-based procedure for the detection of gullies is the derivation of the first three aforementioned indices (*nTPI*, terrain slope, and terrain roughness). The fourth index (length to width ratio) will be derived at a later stage, since it first requires a further operation of segmentation detailed in Section 3.2.1. In particular, for the *nTPI* index, Evans and Lindsay (2010) suggest to choose the kernel size as a function of the typical width of the gullies to detect. In order to determine the best kernel size to detect gullies, *nTPI* was derived at three different kernel sizes, equal to 10, 20, and 30 m, respectively. The four indices previously defined have been used within the software *eCognition developer 9.2* for the detection of gullies (bottom and boundaries). The software provides a collection of tools for GEOBIA, facilitating the classification of images in various application fields (e.g., remote sensing).

The second step consists of using the *nTPI* layer within *eCognition developer 9.2* as starting layer to apply the segmentation process, which is the main process of *OBIA* (Hay and Castilla, 2008), in order to derive homogeneous pixel clusters (also called segments or objects) that provide the base layer for the following analysis steps. Among the variety of segmentation algorithms, here it was decided to use the *Multi-Resolution segmentation* algorithm (Baatz and Schape, 2000). It is a bottom-up approach that aims to merge neighbor pixels having a heterogeneity parameter less than a specific threshold, fixed by the user. This leads to the creation of segments to whom is assigned the same class during the following classification process. Compared to the classical pixel-based approach, this process leads to a number of elements to process lower than that of pixels that make the original image and, for this reason, easier and faster to be analyzed. The optimal values of parameters, in order to obtain the segments from the original image, have been defined through a calibration procedure of segmentation detailed in Section 3.2.1.

A final phase of classification, based on different aspects of objects, such as spectral or textural attributes, allows the user to classify images and recognize a landform in the landscape (e.g., gullies in the present study). A *developed rulesets* section allows the user to set up an ensemble of rules aiming to automate the process and replicate it on different areas. A section called *Image Object Information* enables the user to query and get the values of some specific variables within an object and use them to set up a process tree of rules and/or algorithms aimed to detect a given object (e.g., gullies).

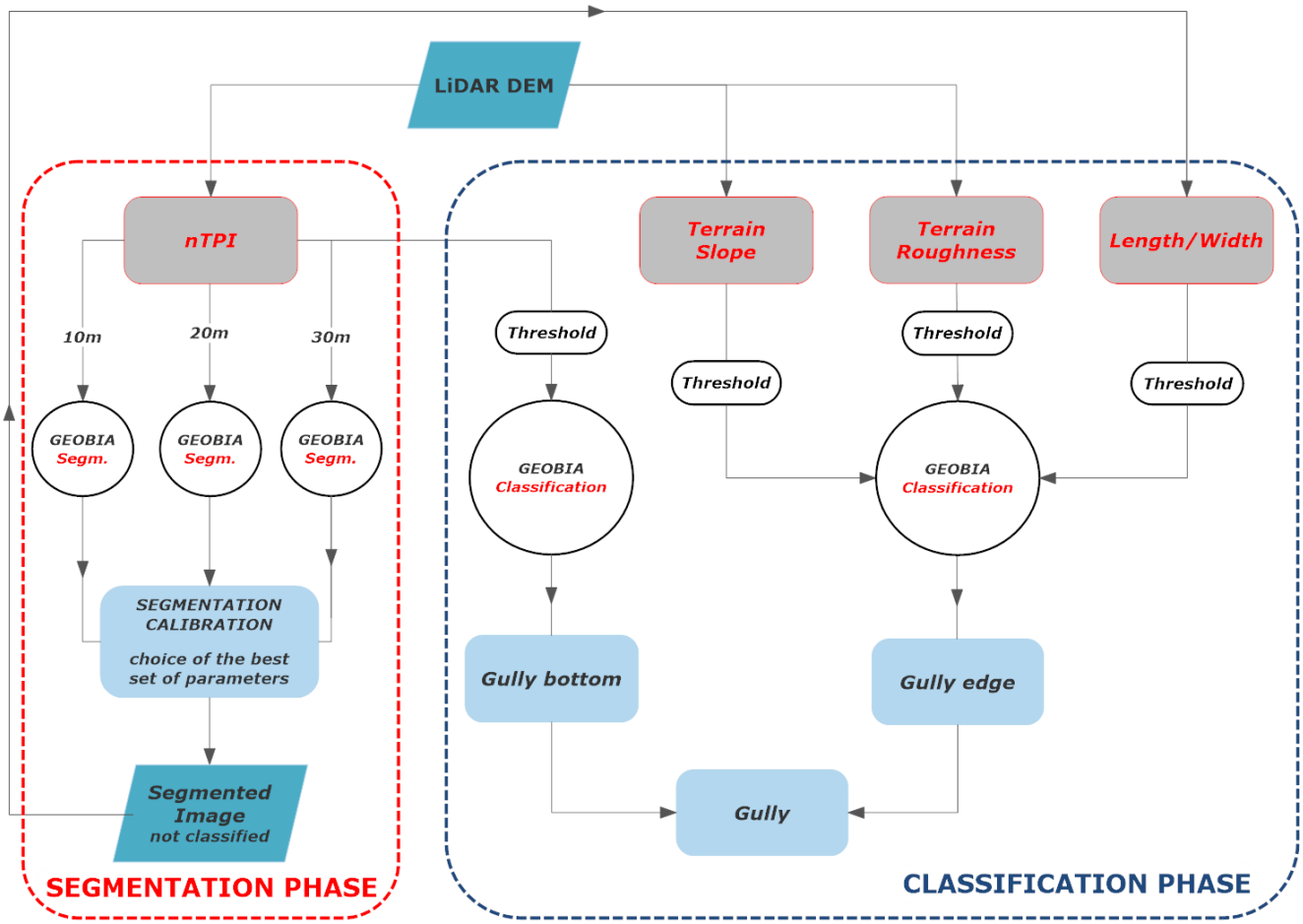

Figure 2 - Flow chart of proposed gully detection procedure

3.2.1. The *Multi-Resolution segmentation* algorithm

Segmentation creates segments or objects representing features that may be spectrally variable at the level of the single pixel. The most important parameter in order to identify homogeneous objects is the *scale parameter*, *e*, consisting of the maximum heterogeneity, or degree of fitting, between two neighbor pixels or objects. As the *scale parameter* increases, the number of merged pixels into a single object or the number of merged objects into a bigger object increases as well. On the contrary, as the *scale parameter* decreases, the original image will be fragmented into a higher number of small objects.

According to Baatz and Schape (2000), considering two objects within the same *d*-dimensional feature space (i.e., the layer or the ensemble of layers used to perform the multi-resolution segmentation), the degree of fitting indicates the heterogeneity, *h*, between the two objects in that

feature space, calculated through equation (3), where the terms f_{1d} and f_{2d} stand for the values of the two objects in that feature space:

$$h = \sqrt{\sum_d (f_{1d} - f_{2d})^2}. \quad (3)$$

Actually, the similarity between two adjacent objects is evaluated as a function of a spatial and a spectral component (Happ et al., 2010). The first one depends on the shape of the objects, while the second one is related to the spectral response of the pixels within the objects. Since the process is bottom-up, the process starts at the pixel-level; in this case, the pixels represent the segments. At the first step the algorithm calculates the heterogeneity between a selected pixel and all its neighboring as a *fusion factor*, *f*, in equation (4). The merging operation is performed between the selected pixel and the one having the lowest *fusion factor*, but only if it is less than the *scale parameter*, having the role of a threshold previously fixed by the user. At the second step the same process is repeated considering the segments resulting from previous step. The process will be repeated up to reach the final segmentation, when the heterogeneity between every segment of the final image and all its neighboring segments is greater than the *scale parameter*:

$$f = w_{color} \cdot h_{color} + (1 - w_{color}) \cdot h_{shape}. \quad (4)$$

In equation (4) the spectral heterogeneity, h_{color}, and the spatial heterogeneity, h_{shape}, are weighted by the term w_{color} and its complementary to one, w_{shape}, respectively. The spectral heterogeneity can be obtained through equation (5):

$$h_{color} = \sum_i w_{color} \cdot (n_{obj3} \cdot \sigma_c^{obj3} \cdot (n_{obj1} \cdot \sigma_c^{obj1} - n_{obj2} \cdot \sigma_c^{obj2})), \quad (5)$$

where the index *obj3* represents the object resulting from the merging operation between the selected segment (*obj1*) and the neighboring segment (*obj2*). Therefore, the equation (5) shows that h_{color} depends on the number of pixels included in the three analyzed objects (n_{obj3}, n_{obj1} and n_{obj2}) and also on the standard deviation of the spectral response for a generic band *c* (σ_c) of all the pixels belonging to those segments.

The spatial heterogeneity depends on the shape of the objects and is calculated by using equation (6), as a function of the compactness, h_{cmpct}, and the smoothness, h_{smooth}, factors. The terms h_{cmpct} and h_{smooth} are weighted by w_{cmpct} and its complementary to one, w_{smooth}, respectively.

$$h_{shape} = w_{cmpct} \cdot h_{cmpct} + (1 - w_{cmpct}) \cdot h_{smooth}. \quad (6)$$

For each object the compactness factor, h_{cmpct}, can be calculated by dividing its perimeter by the square root of the number of pixels within it, while the smoothness factor, h_{smooth}, as the ratio between its perimeter and the perimeter of the box bounding the object.

That being said, considering the perimeter of the object as a constant value, as the h_{cmpct} grows the number of pixels within the object decreases, leading to thinner and less compact segments. In the same way, fixing a constant rate of the length of the boundary box, as the h_{smooth} increases the segments tend to become longer and thinner. In order to perform the *Multi-Resolution segmentation* algorithm, it is necessary to input in *eCognition developer 9.2* the weights w_{shape} and w_{cmpct} related to the spatial and spectral heterogeneities, respectively.

One way to optimize the values of above parameters is to calibrate the segmentation procedure (Clinton et al., 2010; Liu et al., 2017; Liu et al., 2012). According to Liu et al. (2012), the overlay between the reference polygon (e.g., the actual gullies boundaries) and the corresponding segments could generate under-segmented and over-segmented areas, apart from the overlapped areas (Figure 3). As it is possible to see in Figure 3, in the relationships between the reference polygons (continuous line in Figure 3) and the corresponding segments (dashed line in Figure 3) can be: one-to-many, one-to-one, and many-to-one.

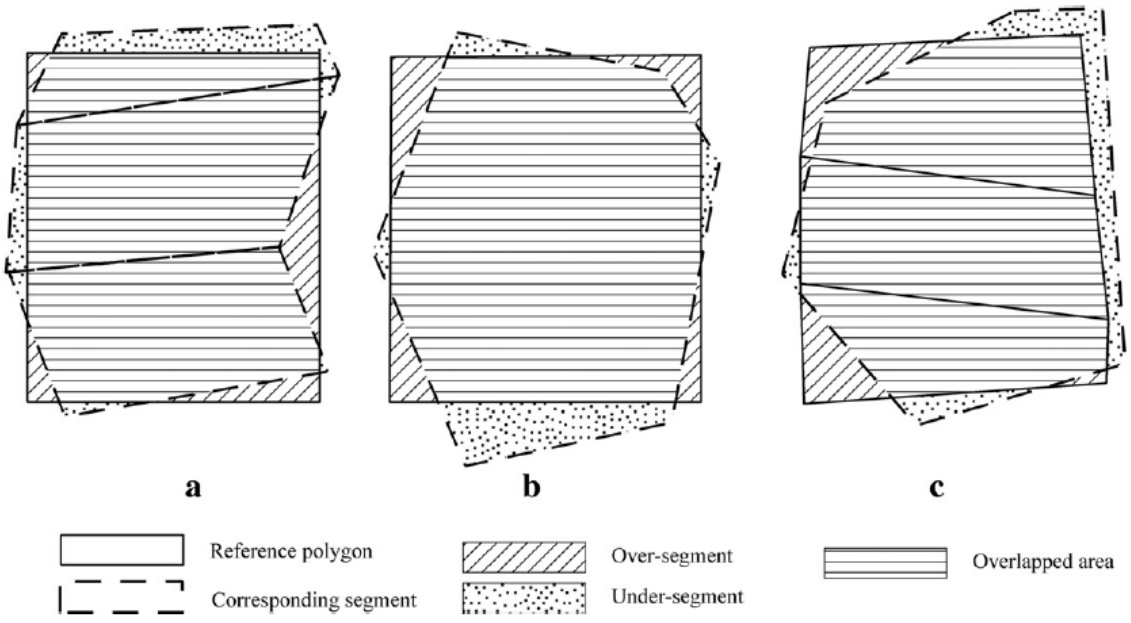

Figure 3 - Comparison between the reference polygon and the corresponding segments. (a) displays the one-to-many relationship, (b) the one-to-one and (c) the many-to-one. Figure from Liu et al. (2012).

According to the schemes depicted in Figure 3, it is possible to affirm that the goodness of the *Multi-Resolution segmentation* result, as far as concerned the geometric relationships, can be measured through the following three metrics:

$$OS = \frac{\sum|r_i - s_k|}{\sum|r_i|}, \tag{7}$$

$$US = \frac{\sum|s_k - r_i|}{\sum|s_k|}, \tag{8}$$

$$ED_1 = \sqrt{\frac{OS^2 + US^2}{2}}. \tag{9}$$

In equations (7) and (8) the term r_i stands for the reference polygon and the term s_k represents the segment that has to be compared with the reference polygon. In general, equation (7) provides the *Over-Segmentation* factor (OS), because it sums up the areas included in the reference polygon but not in its corresponding segments. The output given by equation (8) is the *Under-Segmentation* factor (US), since it is representative of all those pixels included in the segments, but that are outside the reference polygon. Besides, the output provided by equation (9) is the *Euclidean Distance* 1 (ED_1) and is the distance from the perfect geometric segmentation result. By analyzing the equations (7), (8), and (9), it is easy to affirm that in the ideal case of perfect match between the reference polygon(s) and the segment(s) all the three metrics should be equal to zero. The over-segmentation and the under-segmentation are two of the main limitations of object-based approach of images (Figure 3), which can affect the subsequent classification process in two ways: i) under-segmentation results in image objects that cover more than one class and thus introduce classification errors because all pixels in each mixed image object have to be assigned to the same class and ii) features extracted from images affected by over-segmentation or under-segmentation do not represent the properties of real objects on the Earth such as shape and/or area (Liu and Xia, 2010)

In order to take into account the arithmetic relationships as well, Liu et al. (2012) proposed the following new indices:

$$PSE = \frac{\sum|s_i - r_k|}{\sum|r_k|}, \tag{10}$$

$$NSR = \frac{|m - v|}{m}, \tag{11}$$

$$ED_2 = \sqrt{PSE^2 + NSR^2}. \quad (12)$$

where *PSE* and *NSR* stand for *Potential Segmentation Error* and *Number of Segment Ratio*, respectively, while *m* and *v* represent the number of reference polygons and the number of corresponding segments, respectively. ED_2 is the *Euclidean Distance* 2 and measures the distance from the perfect arithmetic segmentation.

In order to come up with a single index value that took into account both the geometric and arithmetic segmentation results, the ED_1 and ED_2 have been combined into the key performance indicator, *KPI* (Goepel, 2018), of equation (13):

$$KPI = \sum_{i=1}^{k} w_i \cdot IC_i, \quad (13)$$

where k=2 (i.e., ED_1 and ED_2), w_i is the weight of IC_i, here assumed equal to 0.5 for both ED_1 and ED_2, and IC_i is calculated by means of equation (14):

$$IC_i = 100 \cdot \frac{PI_i - base_i}{target_i - base_i}, \quad (14)$$

where PI_i is the value of the i^{th} index (i.e., ED_1 and ED_2), $base_i$ is the value indicating the worst performance of the i^{th} index and $target_i$ is the value indicating the best performance of the i^{th} index (i.e., zero for both ED_1 and ED_2). The *KPI* ranges between 0 and 100, whit 100 indicating a perfect match in terms of geometric and arithmetic results.

3.2.2. The object-based *Classification*

Object-based classification involves categorization of pixels on the base of the spatial relationship with the neighboring pixels. Differently from the pixel-based classification, the object-based classification attempts to mimic what the human eyes do during visual interpretation basing on the spectral properties (i.e., color), size, shape, and texture of objects obtained with the segmentation.

The process relies on the construction of one or more rules sets that can be used in cascade across a variety of layers to classify the segments resulted from the *Multi-Resolution segmentation* algorithm; such a procedure allows the user to produce a repeatable methodology. Depending on the purpose of the classification, it is possible to set different kinds of rules. As an example, some

rules aim to classify objects on the base of a threshold. In this case, the threshold value can be calibrated on the base of literature indications or, in the absence of those, querying the values of some specific variables within objects falling within an interest area. Some other rules can be written up on the base of adjacency or distance between segments.

The software *eCognition developer 9.2* allows the user to create different rules working with one or more layers, since they can be linked through logical *or* and *and* operators. Each rule can be independent from the others or linked to them in a cascade of rules, where each rule operates on the classified segments from the previous ones.

As it is possible to understand from the above considerations, a good classification requires a good a priori knowledge of the area and the types of land cover under investigation, which may not necessarily be available. Further, there is no definitive algorithm or parameters for the creation of image objects.

4. Method setup and calibration: application to the SUBAREA-A

Following the approach proposed by Clinton et al. (2010) and later applied by Liu et al. (2017) to identify gullies in the Yaojiawan catchment (Shaanxi Province, China), the proposed method has been previously calibrated on the two surveyed gullies of SUBAREA-A already shown in Figure 1. Such an optimization process is very convenient, since enables to compute segments fitting the actual boundaries of the two considered gullies in the most proper way.

The proposed methodology involves making choices of many different parameters, which may influence the resulting outcome in terms of accuracy of the identification of gullies. Main choices regard the *nTPI* kernel, α, and the segmentation parameters (i.e., e, w_{shape}, and w_{cmpct}). With reference to the *nTPI*, three different kernel sizes (i.e., 10, 20, and 30 m) were fixed a priori on the base of a simple qualitative visual analysis and considering that the two gullies of the SUBAREA-A have both a width of about 20m. With reference to the segmentation parameters, instead, a certain range of variability for the *scale parameter* (i.e., 3, 5, 10, and 20) and the weights related to the spatial heterogeneity and the compactness factor has been explored. More in details, w_{cmpct} has been set equal to 0.2, 0.45, and 0.9, while w_{shape} equal to 0.2, 0.6, and 0.9.

The *KPI* (see Section 3.2.1) has been used to obtain the set of parameters that provides the best segmentation and the confusion matrix to evaluate the goodness of the final classification.

4.1.1. Multi-Resolution segmentation

Based on morphology and most common shape of gullies, the expected result of segmentation should have thin and long segments in correspondence of the gully-affected areas and more compact segments outside them. Considering what said in Section 3.2.1, once fixed the *scale parameter*, *e*, these results should be obtained for low weights of the spatial heterogeneity and compactness factor.

In order to perform the *Multi-Resolution segmentation* algorithm, the only layer of the *nTPI* has been used. In order to calibrate the process, a number of 108 possible combinations resulting from the considered ranges of variability of *nTPI* (3), *e* (4), w_{shape} (3), and w_{cmpct} (3) have been considered by setting up an ensemble of segmentation attempts and evaluating, for each of them, the goodness of the results in terms of *KPI*. The results of calibration, here not shown for the sake of brevity, demonstrated that the more suitable size for the kernel of the *nTPI* was 30 m (hereafter *nTPI*30). With reference to the two gullies of SUBAREA-A, a visual inspection of *nTPI*30 layer seems to ensure that pixels belonging to the gully-affected areas, either bottom or edges, and to the gully not-affected areas are likely to be included in the same kernel. In terms of *Multi-resolution segmentation*, this means that all the pixels covering the bottom of a gully are likely merged into objects with strongly negative values of *nTPI*30 while; similarly, the edges of gullies are merged into objects still having negative values of *nTPI*30 but closer to zero than the object representing the bottom. Figure 4 shows the 36 possible combinations and their results in terms of KPI for the segmentation obtained with the *nTPI*30 (circles in Figure 4). In order to explore how the segmentation performance varies within the space of parameters, the KPI values have been interpolated with the *IDW* method in QGIS maintaining constant the *scale parameter*.

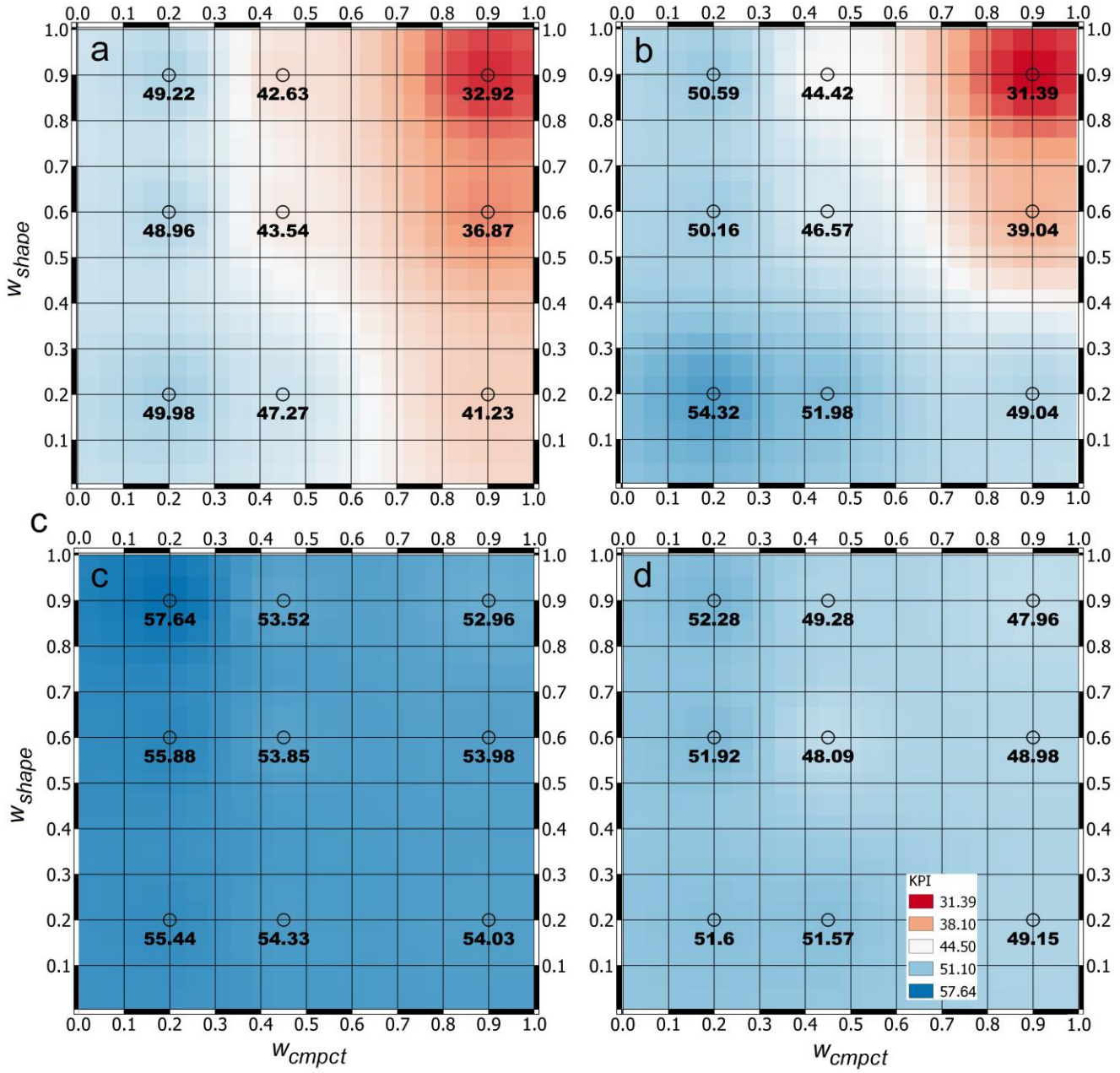

Figure 4 – Results of the Multi-Resolution segmentation in terms of punctual and interpolated KPI values for nTPI = 30 m and a) e=3, b) e=5, c) e=10, and d) e=20.

As it is possible to observe in Figure 4, theoretically, the best segmentation results correspond to e = 10 and lower values of w_{cmpct} (Figure 4c). Actually, looking at the values of ED_1 and ED_2 for e=10, here not shown for the sake of brevity, it is possible to notice that at the high values of *KPI* correspond high values of ED_1 and low values of ED_2, which mean for what said in Section 3.2.1, that there is a good arithmetic segmentation but not a good geometric segmentation. This is mainly due to a high under-segmentation rate. In this case, the image is fragmented in a very low number

of wide *segments*. This situation is even more exacerbated in the case of *e*=20 (Figure 4d). Moreover, from the observation of Figure 4, it is possible to notice a higher variability of *KPI* for lower values of *e* (i.e., higher sensibility of *KPI* to w_{cmpct} and w_{shape}).

On the contrary, looking at the Figures 4a and 4b it is possible to notice a higher variability of *KPI* in the ranges of w_{shape} and w_{cmpct}. In both the cases, the segmentation performance, in terms of *KPI,* get worse when w_{shape} and w_{cmpct} grow together. In these cases, looking at the values of ED_1 and ED_2, it is possible to notice that there is a good geometric segmentation (i.e., low values of ED_1) but not a good arithmetic segmentation (i.e., very high values of ED_2). In fact, the combination of high values of w_{shape} and w_{cmpct} along with low values of the *scale parameter* leads to a very fragmented image, tending to the pixel-based approach in the extreme case, which means a very good match in term of geometry but not in terms of number of segments.

According to Baatz and Schape (2000), who assert that "*no segmentation result - even if quantitatively proofed - will convince, if it does not satisfy the human eye*", in order to decide the combination of *e*, w_{shape}, and w_{cmpct} to use for the segmentation, we also evaluated the visual match between objects and surveyed gullies shape. Figure 5 shows the comparison between the segmentation for the case *e* = 10, w_{shape} = 0.9, and w_{cmpct}= 0.2, which is the best result in terms of *KPI*, and the case *e* = 5, w_{shape} = 0.2, and w_{cmpct}= 0.2 that, not considering the results for *e* = 10, is the best result obtained in terms of *KPI* (i.e., 54.32 in Figure 4b). In particular, Figures 5a and 5b show the results of segmentation in correspondence of the two surveyed gullies of SUBAREA-A relatively to *e* = 10, w_{shape} = 0.9, and w_{cmpct}= 0.2, while Figures 5c and 5d show the results of segmentation for *e* = 5, w_{shape} = 0.2, and w_{cmpct}= 0.2. The image segments displayed in Figures 5 are only those intersecting the actual gully-affected areas.

It is possible to notice in Figure 5 that, as the *scale parameter* increases, the size of objects increases as well. Looking at the Figures 5a and 5b (*e* = 10), segmentations resulted into a low number of large objects leading to high values of *OS* and/or *US* and, consequently, higher values of ED_1. More importantly, there is a coarse segmentation inside the actual gullies that could result in a raw classification. The opposite considerations can be made by observing the Figures 5 c and 5d, where e = 5. In this case, a higher number of long and narrow objects allows for a better description of geometry but a worse segmentation in terms of arithmetic results.

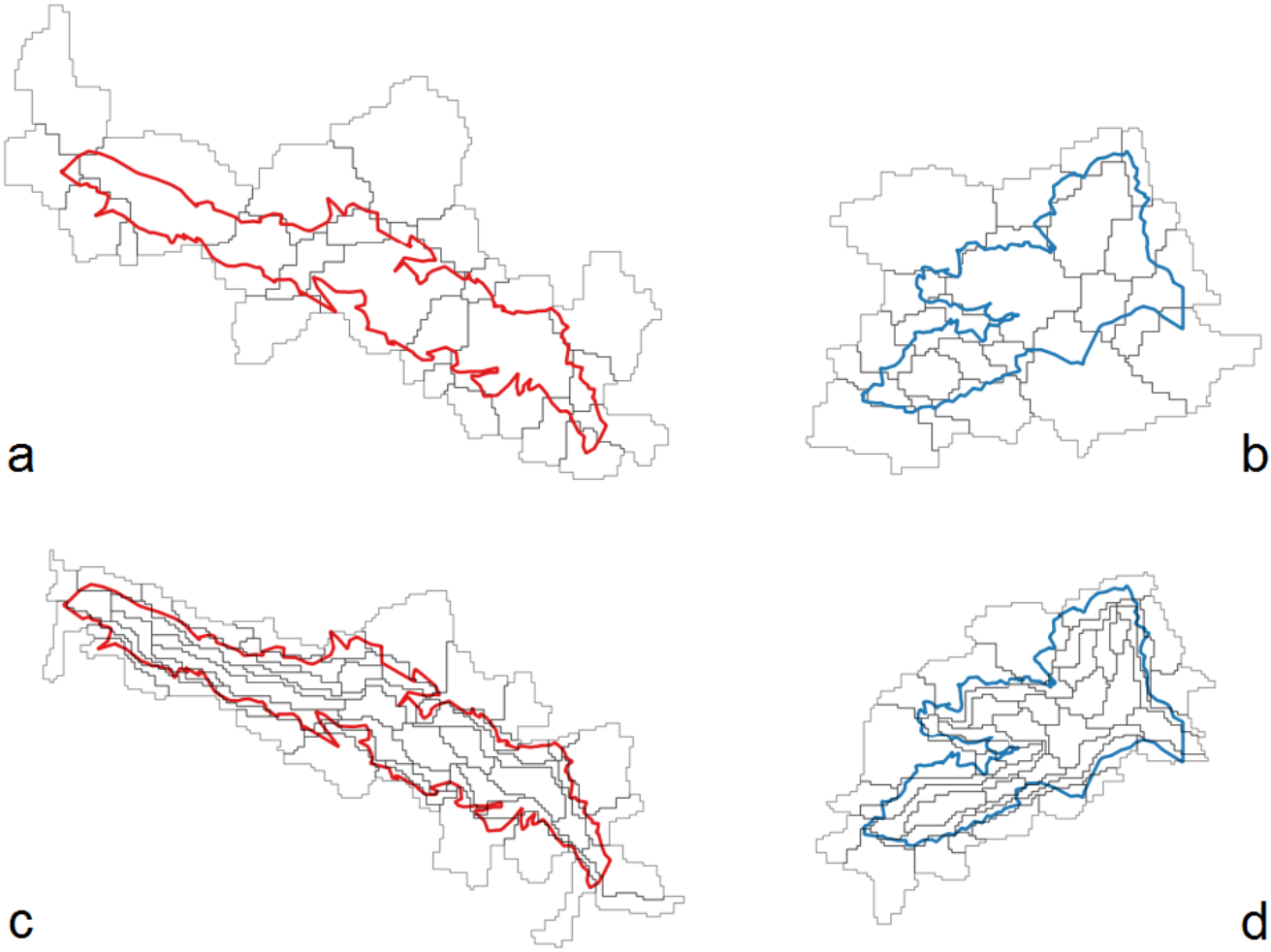

Figure 5 - Segmentation results for e = 10, $\boldsymbol{w_{shape}}$ = 0.9, and $\boldsymbol{w_{cmpct}}$ = 0.2 for the a) left basin and the b) right basin and e = 5, $\boldsymbol{w_{shape}}$ = $\boldsymbol{w_{cmpct}}$ = 0.2 for the c) left basin and the d) right basin. Black lines indicate segmentation.

Considering the previous arguments, according to Baatz and Schape (2000) it has been decided to select the following values for the segmentation of SUBAREA-A: e = 5, w_{shape} = w_{cmpct} = 0.2. Starting from this segmentation has been possible to retrieve different information at the segment scale, among which the length to width ratio, useful for the next step of classification.

4.1.2. Classification

Figure 6 shows the two surveyed gullies of SUBAREA-A overlaid to the spatial distributions of the four indices above mentioned: *nTPI*30 (Figure 6a), terrain slope (Figure 6b), terrain roughness (Figure 6c), and length to width ratio (Figure 6d). Looking at the Figure 6a, as already discussed in

Section 4.1.1, it is possible to notice that the objects belonging to the bottom of gullies are characterized by negative values (blue color in Figure 6a), while edges are identified by still negative values but closer to zero (yellow color in Figure 6a). By observing the slope and the terrain roughness, shown in Figures 6b and 6c, respectively, it is clear that the higher values of both these variables are in correspondence of gullies edges (red color in both Figures 6b and 6c). Finally, from the Figure 6d, it is possible to see that if the element is tiny and long, as gullies usually are, has high values of length to width ratio (yellow to red color in Figure 6b).

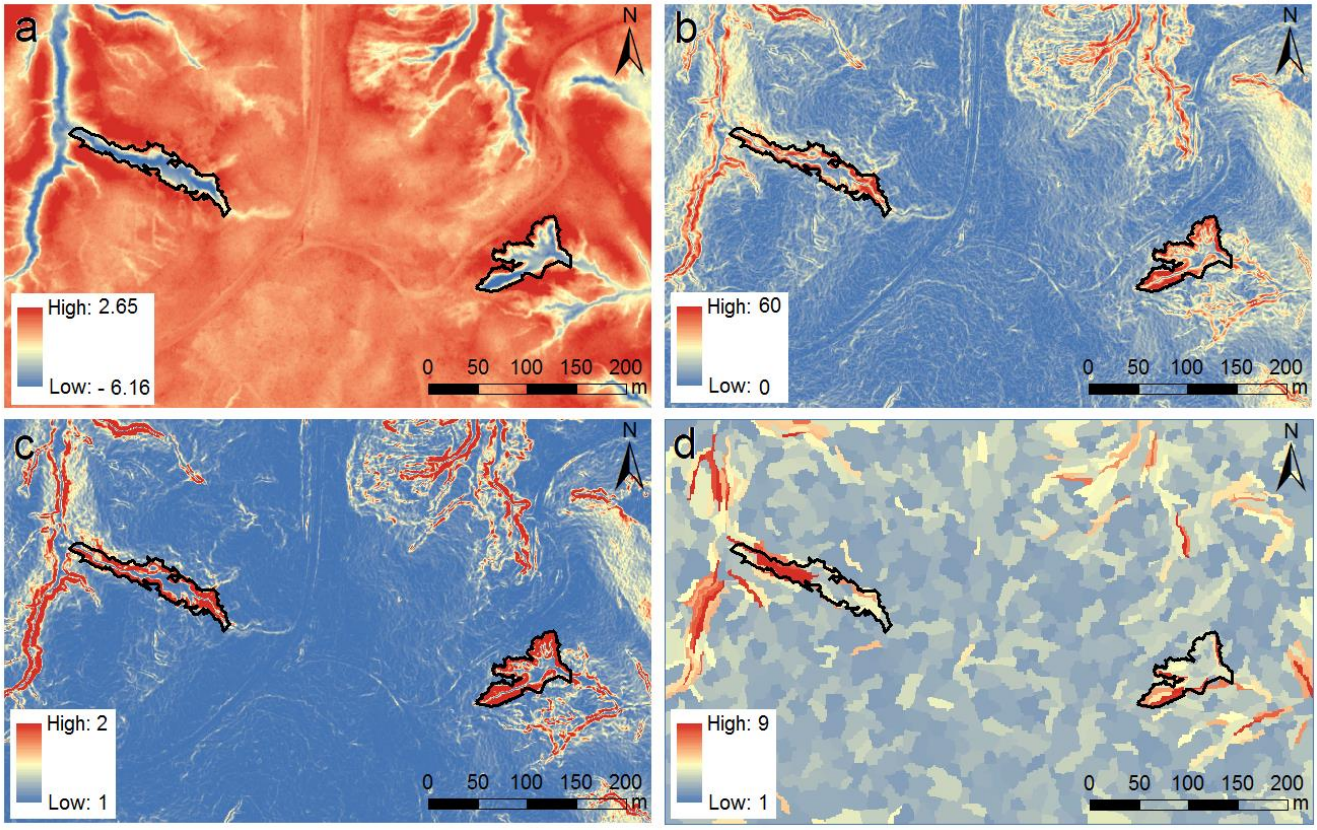

Figure 6 - Spatial distribution of the four indices used to detect gully bottom and edges: a) TPI30, b) slope, c) terrain roughness, and d) length to width ratio.

Starting from information contained within the segmented objects that, differently from the classical pixel-based approach, can concern also the values of min, max, mean, standard deviation, etc., of a given variable, we tried to detect landforms connected to gullies. Investigation of previous layers allowed to set up an ensemble of rules and algorithms to detect the bottoms and the edges of the two surveyed gullies of SUBAREA-A.

First of all, we identified the bottom of gullies by using the *nTPI* layer. As already said in Section 3.1.1, low values of *TPI* indicate a cell at or near the bottom of a valley that is likened to the bottom of a gully. That being said, by querying the mean value of *nTPI*30 for both those segments within and outside the surveyed gullies, it was possible to identify and calibrate the value of a threshold, T_1, distinguishing between bottom and other landforms.

Once identified the bottom part of gullies within the SUBAREA-A, for the identification of edges, a similar process led to the identification of three thresholds (i.e., T_2, T_3, and T_4) for the terrain slope, terrain roughness, and length to width ratio layers, respectively.

By means of a Boolean process it was possible to discriminate between elements belonging to a gully and not.

This process resulted in the writing of equation (15), which is the first rule of the cascade process, for the identification of bottom, and equation (16) for the identification of edges:

$$Mean\ (nTPI30) < T_1, \tag{15}$$

$$\begin{cases} Mean\ slope > T_2 \\ Mean\ roughness > T_3. \\ Length/width > T_4 \end{cases} \tag{16}$$

Equation (15) affirms that, for each segment, if the average *nTPI*30 within the object is less than T_1 it is classified as a gully bottom. Equation (16) puts three different conditions together through an *and* spatial operator and, therefore, it represents an intersection. For this reason, only those objects where all of the three conditions are contemporary satisfied are classified as gully edges. In particular, from previous analysis, values of T_1, T_2, T_3, and T_4 resulted to be equal to -2, 20°, 1.15, and 1.5, respectively.

All the segments classified as bottom or edges have been merged into a single class labeled *gully*, while all the unclassified objects have been assigned to a class labeled *non-gully*. The boundaries of the two surveyed gullies, highlighted in continuous black line, overlaid to the classification results (red polygons) are shown in Figure 7.

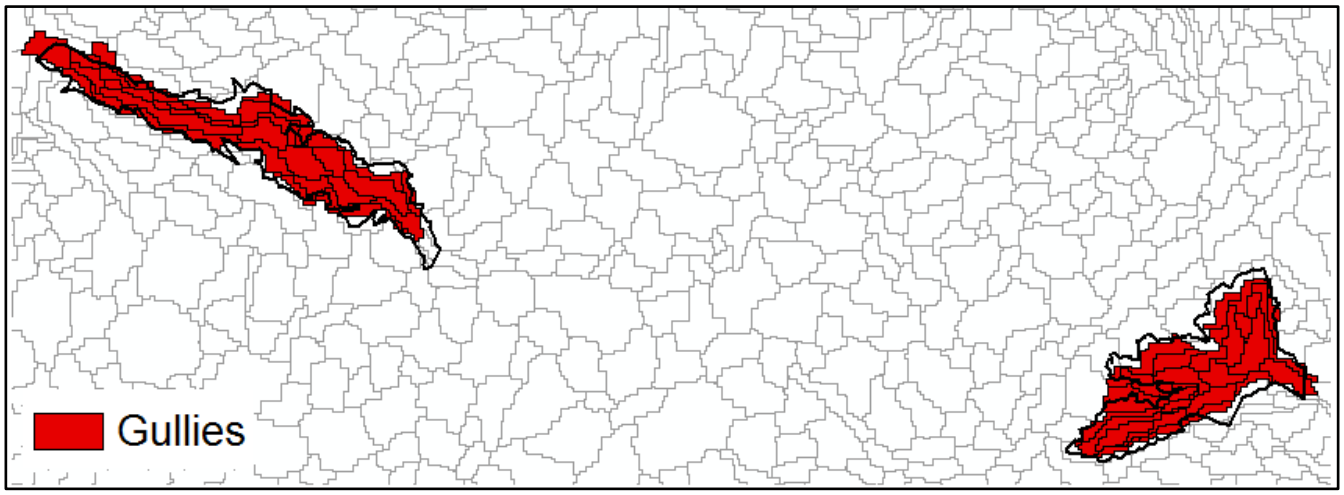

Figure 7 - Results of the classification procedure for the SUBAREA-A after applying equations (15) and (16).

In order to verify the goodness of the achieved classification, the *Accuracy Assessment* tool provided by *eCognition developer 9.*2 has been used for the same two rectangular frames surrounding the two gullies of SUBAREA-A retrieved by Noto et al. (2017) (see Box-SX and Box-DX Figure 2a of Noto et al. (2017)). The tool returns the *overall*, the *user*, and the *producer accuracies* for the classes *gully* and *non-gully* and the *K-index* for both the two classes and takes into account all of the pixels contained into an object. In particular, the overall accuracy is the percentage of pixels correctly classified over the total number of them in the confusion matrix. The user accuracy, for each class, can be obtained through the ratio between the total number of pixels correctly classified and the total number of pixels associated to that class. The producer accuracy, for each class, is measured through the ratio between the total number of pixels correctly classified and the total number of pixels actually included in that class. The *K-index*, finally, takes into account the fact that a random classification returns overall, user, and producer accuracies values greater than zero. From the conceptual point of view, it measures the difference between the probability of correct classification and the probability of correct classification achieved by chance. Once the confusion matrix is completed, *K-index* can be calculated through the equation (17):

$$K = \frac{N \cdot A - B}{N^2 - B}, \tag{17}$$

where the term N stands for the total number of pixels in the confusion matrix, the term A represents the total number of pixels correctly classified, calculated as the sum of the elements in

the diagonal of the confusion matrix and the term *B* indicates the cumulative sum of the products between the total number of pixels in the rows and those in the columns.

The results of accuracy for the left gully and the right gully of SUBAREA-A are shown in Table 1, in the form of confusion matrix, computed as a comparison between the classified image (Figure 7) and a reference image, i.e., a Boolean mask having the value 1 in correspondence of the surveyed gullies and the value 0 elsewhere. As it is possible to notice in Table 1, the tool is able to correctly identify 2,331 pixels within the class *gully* and 10,821 pixels within the class *non-gully*, while it generates 251 false positive and 468 missed correct classifications for the left gully. Moreover, the producer accuracy for the left gully is high for both the two classes, indicating that more than the 83% of the area of the surveyed gullies and almost the 98% of the area not-affected by gullies have been correctly classified. Similar results have been obtained also for the right gully (Table 1). In particular, the tool is able to correctly identify 2,422 pixels within the class *gully* and 5,457 pixels within the class *non-gully*, while it generates 230 false positives and 591 missed correct classifications for the left gully. The producer accuracy for the right gully is high for both the two classes, indicating that about the 80% of the area of the surveyed gullies and about the 96% of the area not-affected by gullies have been correctly classified. The overall *K-index* (calculated on both the Box-SX and Box-DX) resulted equal to 0.816 that is a little bit lower than that calculated by Noto et al. (2017), which was equal to 0.876, thus demonstrating a good performance of the developed procedure.

Since the overall accuracy is very satisfactory (almost the 95% for the left gully and 91% for the right gully), in order to test the procedure developed for the SUBAREA-A, the same rules here discussed have been applied to detect gullies in the SUBAREA-B.

Table 1 - Results for the left gully of SUBAREA-A provided by the Accuracy Assessment tool of eCognition developer 9.2.

User\Reference	**LEFT Gully**			**RIGHT Gully**		
	Gully	Non-gully	Sum	Gully	Non-gully	Sum
Gully	2,331	251	2,582	2,422	230	2,652
Non-gully	468	10,821	11,289	591	5,457	6,048
Sum	2,799	11,072		3,013	5,687	
Accuracy						
Producer	0.833	0.977		0.803	0.959	
User	0.903	0.958		0.913	0.902	
K-index per class	0.794	0.878		0.718	0.867	

Totals						
Overall Accuracy	0.948			0.906		
K-index	0.834			0.786		

4.2. Application of the developed procedure to the SUBAREA-B

As said in Section 4.1.2, since the accuracy assessment related to the SUBAREA-A is satisfying, the same classification rules have been applied to detect the gullies within the SUBAREA-B. Because of the greater extension and the more complex morphology of the SUBAREA-B, as compared to the SUBAREA-A, in addition to the developed rules for the SUBAREA-A, other rules have to be used in order to exclude some morphological features (e.g., some parts of hydrological network and the bank erosion areas) which, at the watershed scale, can be erroneously classified as gullies.

In particular, for the correction of those objects belonging to the hydrological network, all of those objects with a mean value of flow accumulation lower than a threshold, T_5, have been correct as *non-gully*. The layer of flow accumulation for the Holcombe's Branch watershed was previously derived from the DEM in QGIS. For the correction of those objects belonging to the bank erosion areas, instead, it was used a distance threshold, T_6, from those elements corrected as hydrological network at the previous step. In this case, all of those segments with a distance from the hydrological network lower than T_6 have been correct as *non-gully*. This process resulted in the implementation of two new rules in *eCognition developer 9.2*:

$$Mean\ (Flow\ Accumulation) > T_5, \tag{18}$$

$$Distance\ to\ hydrological\ network < T_6. \tag{19}$$

In particular, investigation of objects belonging to the river network and to the bank erosion areas led to set $T_5 equal\ to$ 4,000 pxl and $T_6 equal\ to$ 30 pxl.

In this case, since a spatial distribution of the digitalized actual gullies is not available, in order to assess the appropriateness of the developed procedure, the spatial map of results for the object-based procedure and the pixel-based procedure, developed for the same area by Noto et al. (2017), have been compared (Figure 8).

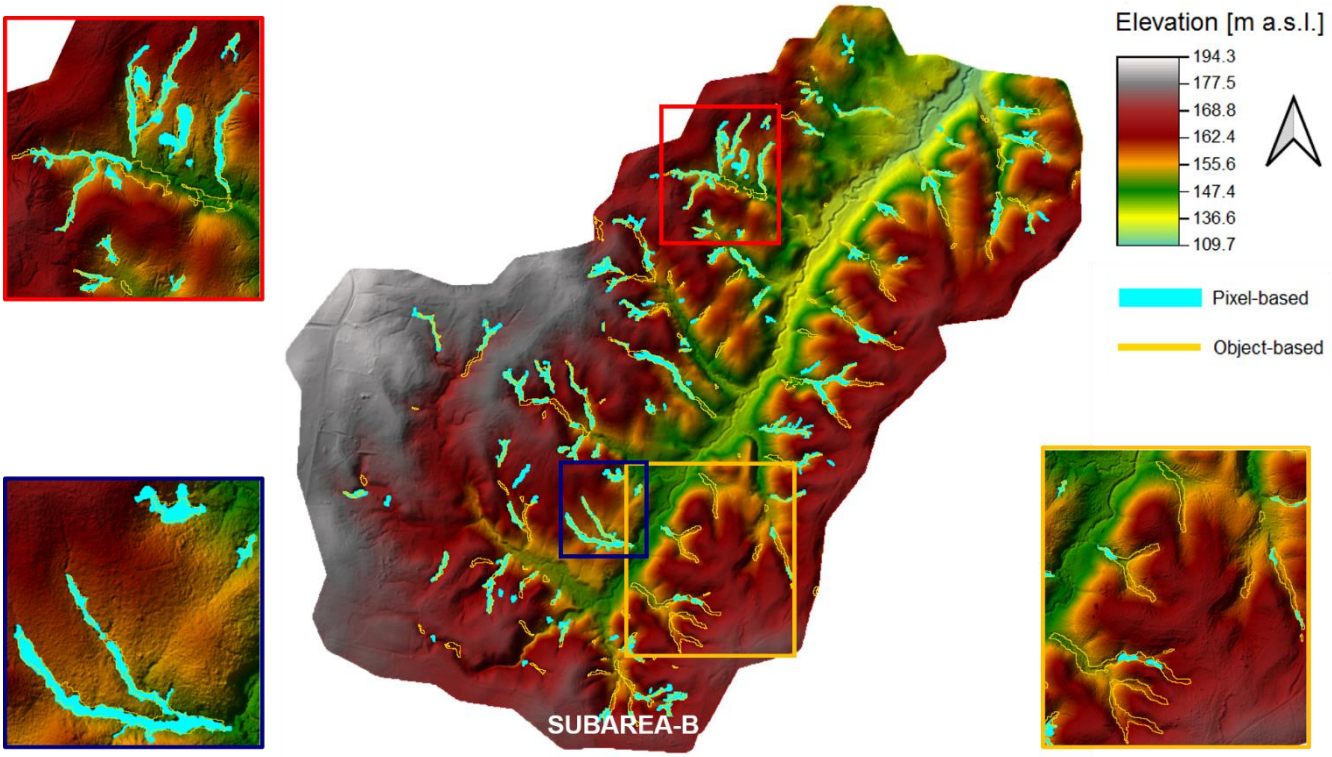

Figure 8 – Comparison between the gullies achieved through a GEOBIA technique (yellow lines) and a pixel-based image analysis (cyan polygons). Boxes yellow, blue, and red show some focuses on the Holcombe's Branch watershed.

From an overview of Figure 8, it is possible to notice that the number of gullies detected with the object-based approach (yellow contours in Figure 8) is higher than that obtained with the pixel-based approach (cyan polygons in Figure 8). Moreover, while in some cases there is almost a perfect match between the gullies detected with the two approaches (see blue boxes in Figure 8), in some other cases the match is only partial (see red box in Figure 8) and in some others there is not a match at all (see yellow box in Figure 8). Rarely the pixel-based approach detects gullies that the object-based approach is not able to identify. However, observing the morphology of the Holcombe's Branch watershed in Figure 8, it seems plausible that the landforms identified by the object-based approach are likely gullies and there is a failure in identifying correctly these landforms from the pixel-based approach.

Starting from the distribution map of the gullies in Figure 8 we derived some indices of the gullies such as the area, the boundary length (i.e., perimeter), and the compactness index, and their empirical distribution function (ecdf, Figure 11). According to Noto et al. (2017), the compactness index was defined as the ratio between the perimeter of the gully and the root square of its area (multiplied by 4π). It ranges between 1.28 (most compact gully) and 5.31 (very elongated gully)

and characterizes the shape of the extracted gullies; more it is close to 1, more the shape of the gully is close to a circle.

A total number of 143 gullies were identified with an area ranging between 20 m^2 and about 10,700 m^2 (Figure 11a), whereas the perimeter ranges from 24 m to about 1,950 m (Figure 11b). The compactness index (Figure 11c) ranges from a minimum of 0.04 (very elongated gullies) to a maximum of about 0.6 (more compact gullies). In order to compare the results of the this study with the results of the pixel-based approach provided by Noto et al. (2017), Figure 9 shows also the ecdf for the area, perimeter, and compactness index returned by that study. As it is possible to notice from Figure 11, apart for the compactness index, which is perfectly overlapped to that from Noto et al. (2017), the object-based approach led to identify more extended gullies (e.g., larger area and perimeter) than the pixel-based approach. This difference is due to the two different approaches and, mainly, to the fact that the object-based approach works with elements, which are aggregation of pixels, where the minimum size of the element is not that of the pixel anymore.

The main statistical characteristics of extracted gullies are listed in Table 2 where measures of variability (standard deviation and coefficient of variation) show the strongest spatial variability of area and perimeter (CV equal to 1.34 and 1.07, respectively) and a greatest homogeneity (low CV) for compactness index.

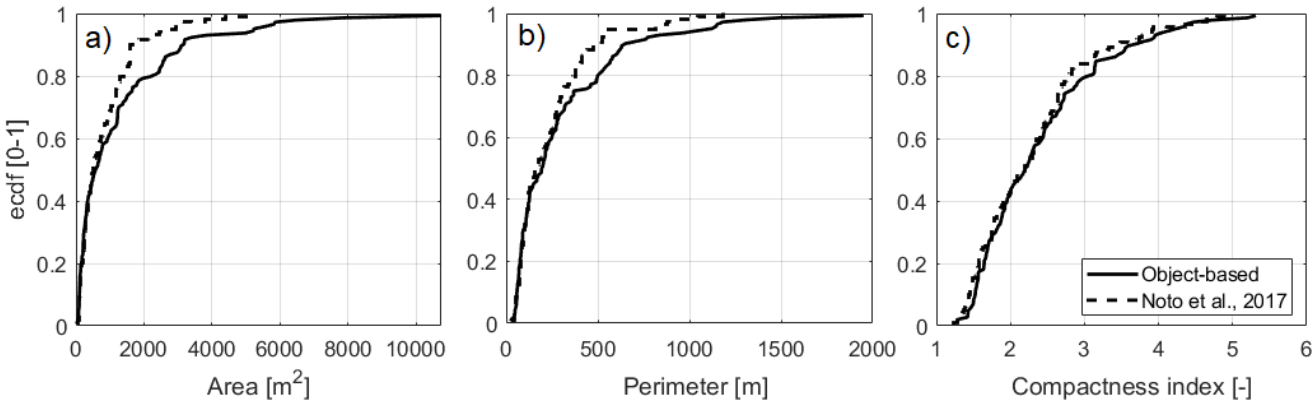

Figure 9 – Empirical cumulative distribution function (ecdf) of morphometric characteristics of gullies identified by the proposed methodology over SUBAREA-B: a) area, b) perimeter, and c) compactness index.

Table 2 - Statistics of classified gullies for SUBAREA-B: minimum, maximum, and mean values (Min, Max, Mean, respectively), standard deviation (STD), and coefficient of variation (CV) of the three gully characteristics.

	Min	Max	Mean	STD	CV
Area [m²]	20.01	10,732.51	1,256.10	1,683.09	1.34
Perimeter [m]	24.01	1,950.68	301.31	320.89	1.07
Compactness Index [-]	1.28	5.31	2.39	0.86	0.36

5. Discussion

Spatial distribution of gullies identified by the object-based approach here developed for the Holcombe's Branch watershed (Figure 8) seems to provide a good definition of the spatial pattern of gullies. The application of the procedure to SUBAREA-B provided the identification of gullies on the base of segmentation and classification previously developed, calibrated, and tested for the SUBAREA-A. Differently than the study of Noto et al. (2017), which removed the main river channel and the bank erosion landforms in the SUBAREA-B manually or by means of a threshold for the gullies area, here we used a couple of rules related to the contributing area and to the distance from the channels, respectively.

In order to minimize the errors due to the over-segmentation and under-segmentation of images (Figure 2) some geometric and arithmetic relationships have been used to calibrate the segmentation on the SUBAREA-A, where two gullies were surveyed during a field survey carried out in June 2015. While the geometric relationship ensures the best match possible in terms of area and shape, the arithmetic relationship ensures the best segmentation in terms of number of objects (i.e., as less objects as possible). The geometric and arithmetic relationships have been combined in a unique index representative of the goodness of segmentation. According to Baatz and Schape (2000), who assert that "*no segmentation result - even if quantitatively proofed - will convince, if it does not satisfy the human eye*", to decide the best parameters to use for the segmentation we also evaluated the fit of the objects with the actual gullies shape of SUBAREA-A. The set of chosen parameters was e = 5, w_{shape} = 0.2, and w_{cmpct}= 0.2. For the classification of objects, a set of rules based on parameters thresholds and/or adjacency or distance from other objects has been used. Since a gully can be usually characterized by a bottom and some edges, which are defined by different characteristics, it has been preferred to set up a rule for the identification of the bottom and three rules in cascade for the identification of the edges. For the first case, we used the $nTPI30$ parameter, while for the edges we used the terrain slope, the terrain roughness, and the length to width ratio.

One of the most important advantages of the proposed method consists in the reproducibility of the developed procedure also for other areas of the Earth, while some limitations of the approach are the fact that parameters, being calibrated using data of manual survey (SUBAREA-A), are

sensitive to the average size of those gullies and, for this reason, they should be recalibrated in areas characterized by gully patterns different from those present in the CCZO study area.

The evaluation process carried out for SUBAREA-A, based on the *Accuracy Assessment* tool provided by *eCognition developer 9.2*, has not be applied to SUBAREA-B because of the lack of data due to the great difficulties related to a complete survey over the entire watershed area. For this reason, only in this case, the physical consistency of the developed procedure has been evaluated by comparing the gullies pattern provided by the proposed method with that of Noto et al. (2017). Even though in some cases the results are not perfectly matching, from the observation of morphology provided with the LIDAR DEM of the Holcombe's Branch watershed it is plausible to say that the GEOBIA procedure is able to detect also gullies, or parts of those, that have not been detected by the pixel-based approach, thus providing to be a reliable tool to identify gullies once the procedure has been calibrated and tested.

The comparison of *ecdf* for some characteristics of the gullies such as the area, the perimeter, and the compactness index (Figure 11) showed that the object-based procedure leads to gullies with bigger ranges of area and perimeter than those identified by Noto et al. (2017). While the difference in terms of upper limits depends on the developed methodology, the different lower limit is mainly due to the fact that, differently from Noto et al. (2017), we did not eliminate from classification those gullies with an area smaller than a given threshold.

6. Conclusions

An object-based approach to detect landforms is presented in this study. The approach, differently from the classical pixel-based approach, uses the characteristics and features of groups of pixels, called objects or segments, to differentiate land cover classes with similar spectral information. As compared to the pixel-based approach, the possibility to consider this extra information gives GEOBIA the potential to produce land cover thematic maps with a higher accuracy.

The GEOBIA has been applied to the Calhoun Critical Zone Observatory (CCZO), an area of South Carolina particularly interesting since characterized by the presence of numerous gullies due to a very intense erosion activity due to the abandonment of terrains used for intensive crop production in the past century.

The software used to carry out the study is the *eCognition developer 9.2*, developed by *Trimble Navigation Ltd*, which provides a collection of tools for OBIA and GEOBIA, facilitating the classification of images in various application fields. The software allows the user to develop a procedure that starts from the segmentation of an image to create groups of homogeneous pixels (also called objects or segments) to whom is assigned the same class during the following classification process. The main advantage of the developed procedure, as compared to a classical pixel-based approach, is that the number of elements to process is highly lower than that of pixels that make the image and, for this reason, easier and faster to be analyzed.

Two areas, the SUBAREA-A and the SUBAREA-B, inside the CCZO have been used to calibrate and test, respectively, the developed procedure. The first area is characterized by the presence of two gullies detected during a field survey in June 2015. The surveyed gullies have been used as reference to calibrate the GEOBIA procedure and thus obtain the optimal segmentation and classification. The procedure, then, has been applied to the SUBAREA-B, corresponding to the Holcombe's Branch watershed, to test the goodness of the developed procedure.

Results showed that the GEOBIA procedure developed in *eCognition developer 9.2* is able to detect gullies with a good accuracy even though, since the absence of surveyed gullies for the SUBAREA-B, the results have been evaluated using as reference the results from a pixel-based approach developed for the same area by Noto et al. (2017).

Although the approach surely requires further test to other gullied systems where good quality topographic data is available, the demonstrated capability of *eCognition developer 9.2* in developing OBIA or GEOBIA procedures to identify gullies in a given area of Earth, coupled with the increasing availability of LIDAR data, allow to say that this automated technique has potential for individuation of different landforms (e.g., landslides) and applications across a range of environments.

References

Baatz, M., Schape, A., 2000. Multiresolution segmentation: an optimization approach for high quality multi-scale image segmentation.

Boardman, J., 2006. Soil erosion science: Reflections on the limitations of current approaches. Catena 68, 73-86.

Clinton, N., Holt, A., Scarborough, J., Yan, L., Gong, P., 2010. Accuracy Assessment Measures for Object-based Image Segmentation Goodness.

D'Oleire-Oltmanns, S., Marzolff, I., Tiede, D., Blaschke, T., 2014. Detection of Gully-Affected Areas by Applying Object-Based Image Analysis (OBIA) in the Region of Taroudannt, Morocco. Remote Sensing 6, 8287.

Eustace, A., Pringle, M., Witte, C., 2009. Give Me the Dirt: Detection of Gully Extent and Volume Using High-Resolution LIDAR, in: Jones, S., Reinke, K. (Eds.), Innovations in Remote Sensing and Photogrammetry. Springer Berlin Heidelberg, Berlin, Heidelberg, pp. 255-269.

Evans, M., Lindsay, J., 2010. High resolution quantification of gully erosion in upland peatlands at the landscape scale. Earth Surf Proc Land 35, 876-886.

Francipane, A., Fatichi, S., Ivanov, V.Y., Noto, L.V., 2015. Stochastic assessment of climate impacts on hydrology and geomorphology of semiarid headwater basins using a physically based model. Journal of Geophysical Research F: Earth Surface 120, 507-533.

Francipane, A., Ivanov, V.Y., Noto, L.V., Istanbulluoglu, E., Arnone, E., Bras, R.L., 2012. TRIBS-Erosion: A parsimonious physically-based model for studying catchment hydro-geomorphic response. Catena 92, 216-231.

Francipane, A., Mussomè, F., Cipolla, G., Noto, L.V., 2018. Object-Based Image Analysis Technique for Gully Mapping Using Topographic Data at Very High Resolution (VHR), in: Goffredo La Loggia, G.F., Valeria Puleo, Mauro De Marchis (Ed.), HIC 2018. 13th International Conference on Hydroinformatics. EasyChair, pp. 725-730.

Goepel, K., 2018. Implementation of an Online software tool for the Analytic Hierarchy Process (AHP-OS). International Journal of the Analytic Hierarchy Process 10, 469-487.

Grosse, P., van Wyk de Vries, B., Euillades, P., Kervyn, M., Petrinovic, I., 2012. Systematic morphometric characterization of volcanic edifices using digital elevation models.

Guisan, A., Weiss, S.B., Weiss, A.D., 1999. GLM versus CCA spatial modeling of plant species distribution. Plant Ecology 143, 107-122.

Happ, P.N., Ferreira, R.d.S., Bentes, C., Costa, G.A.O.P., Feitosa, R.Q., 2010. MULTIRESOLUTION SEGMENTATION : A PARALLEL APPROACH FOR HIGH RESOLUTION IMAGE SEGMENTATION IN MULTICORE ARCHITECTURES.

Hay, G.J., Castilla, G., 2008. Geographic Object-Based Image Analysis (GEOBIA): A new name for a new discipline, in: Blaschke, T., Lang, S., Hay, G.J. (Eds.), Object-Based Image Analysis: Spatial Concepts for Knowledge-Driven Remote Sensing Applications. Springer Berlin Heidelberg, Berlin, Heidelberg, pp. 75-89.

Henderson-Sellers, A., 1994. Land-use change and climate. Land Degradation & Development 5, 107-126.

Huggett, R., 1990. Modelling geomorphological systems edited by M. G. Anderson, John wiley, Chichester 1988. No. of pages: 458. price: $45. 15, 292-293.

Ireland, H.A., Eargle, D.H., Sharpe, C.F.S., 1939. Principles of gully erosion in the Piedmont of South Carolina. U.S. Dept. of Agriculture, Washington.

Jackson, T.J., Ritchie, J.C., White, J., Leschack, L., 1988. Airborne laser profile data for measuring ephemeral gully erosion. Photogrammetric Engineering & Remote Sensing 54, 1181-1185.

James, L.A., Watson, D.G., Hansen, W.F., 2007. Using LIDAR data to map gullies and headwater streams under forest canopy: South Carolina, USA. Catena 71, 132-144.

Jenness, J., 2006. Topographic Position Index (tpi_jen.avx) extension for ArcView 3.x, v. 1.2, 1.2 ed, Jenness Enterprises.

Kirkby, M.J., Cox, N.J., 1995. A climatic index for soil erosion potential (CSEP) including seasonal and vegetation factors. Catena 25, 333-352.

Knight, J., Spencer, J., Brooks, A., Phinn, S., 2007. Large-area, high-resolution remote sensing based mapping of alluvial gully erosion in Australia's tropical rivers. Proceedings of the 5th Australian Stream Management Conference: Australian Rivers: Making a Difference, 199-204.

Liu, D., Xia, F., 2010. Assessing object-based classification: advantages and limitations. Remote Sensing Letters 1, 187-194.
Liu, K., Ding, H., Tang, G., Zhu, A.X., Yang, X., Jiang, S., Cao, J., 2017. An object-based approach for two-level gully feature mapping using high-resolution DEM and imagery: a case study on hilly loess plateau region, China. Chinese Geographical Science 27, 415-430.
Liu, Y., Bian, L., Meng, Y., Wang, H., Zhang, S., Yang, Y., Shao, X., Wang, B., 2012. Discrepancy measures for selecting optimal combination of parameter values in object-based image analysis. ISPRS Journal of Photogrammetry and Remote Sensing 68, 144-156.
Milenković, M., Pfeifer, N., Glira, P., 2015. Applying Terrestrial Laser Scanning for Soil Surface Roughness Assessment. Remote Sensing 7, 2007-2045.
Nearing, M.A., Simanton, J.R., Norton, L.D., Bulygin, S.J., Stone, J., 1999. Soil erosion by surface water flow on a stony, semiarid hillslope. 24, 677-686.
Noto, L.V., Bastola, S., Dialynas, Y.G., Arnone, E., Bras, R.L., 2017. Integration of fuzzy logic and image analysis for the detection of gullies in the Calhoun Critical Zone Observatory using airborne LIDAR data. ISPRS Journal of Photogrammetry and Remote Sensing 126, 209-224.
Pimentel, D., Harvey, C., Resosudarmo, P., Sinclair, K., Kurz, D., McNair, M., Crist, S., Shpritz, L., Fitton, L., Saffouri, R., Blair, R., 1995. Environmental and Economic Costs of Soil Erosion and Conservation Benefits. 267, 1117-1123.
Poesen, J., Nachtergaele, J., Verstraeten, G., Valentin, C., 2003. Gully erosion and environmental change: importance and research needs. Catena 50, 91-133.
Rahmati, O., Tahmasebipour, N., Haghizadeh, A., Pourghasemi, H.R., Feizizadeh, B., 2017. Evaluating the influence of geo-environmental factors on gully erosion in a semi-arid region of Iran: An integrated framework. Science of The Total Environment 579, 913-927.
Ritchie, J.C., Grissinger, E.H., Murphey, J.B., Garbrecht, J.D., 1994. Measuring channel and gully cross-sections with an airborne laser altimeter. 8, 237-243.
Ritter, D.F., Kochel, R.C., Miller, J.R., 2011. Process geomorphology, 5th ed. Waveland Press, Long Grove, Ill.
SCS, 1977. Procedure for determining rates of land damage, land depreciation and volume of sediment produced by gully erosion, in: USDA (Ed.), Guidelines for watershed management, Rome.
Seginer, I., 1966. Gully development and sediment yield. J Hydrol 4, 236-253.
Shruthi, R.B.V., Kerle, N., Jetten, V., 2011. Object-based gully feature extraction using high spatial resolution imagery. Geomorphology 134, 260-268.
Shruthi, R.B.V., Kerle, N., Jetten, V., Abdellah, L., Machmach, I., 2015. Quantifying temporal changes in gully erosion areas with object oriented analysis. Catena 128, 262-277.
Stocking, M.A., 1980. Examination of the factors controlling gully growth. John Wiley and Sons Ltd., Chichester, pp. 505-520.
Tarolli, P., Arrowsmith, J.R., Vivoni, E.R., 2009. Understanding earth surface processes from remotely sensed digital terrain models. Geomorphology 113, 1-3.
Tuckfield, C.G., 1964. Gully erosion in the New Forest, Hampshire. 262, 795-807.
Valentin, C., Poesen, J., Li, Y., 2005. Gully erosion: Impacts, factors and control. Catena 63, 132-153.
Wilkinson, B.H., McElroy, B.J., 2007. The impact of humans on continental erosion and sedimentation. GSA Bulletin 119, 140-156.
Yang, X., Li, M., Na, J., Liu, K., 2017. Gully boundary extraction based on multidirectional hill-shading from high-resolution DEMs. 21, 1204-1216.